# Rayleigh-wave scattering by shallow cracks using the indirect boundary element method



2009 J. Geophys. Eng. 6 221

(http://iopscience.iop.org/1742-2140/6/3/002)

IOP PUBLISHING JOURNAL OF GEOPHYSICS AND ENGINEERING

J. Geophys. Eng. **6** (2009) 221–230 doi:10.1088/1742-2132/6/3/002

# Rayleigh-wave scattering by shallow cracks using the indirect boundary element method

**R Ávila-Carrera[1], A Rodríguez-Castellanos[1], F J Sánchez-Sesma[2] and C Ortiz-Alemán[1]**

[1] Instituto Mexicano del Petróleo, Eje Central Lázaro Cárdenas 152, Gustavo A Madero, México D F, México

[2] Instituto de Ingeniería, UNAM, Circuito Escolar S/N, Coyoacán, México D F, México

E-mail: rcarrer@imp.mx

Received 10 November 2008
Accepted for publication 24 April 2009
Published 29 May 2009
Online at stacks.iop.org/JGE/6/221

**Abstract**

The scattering and diffraction of Rayleigh waves by shallow cracks using the indirect boundary element method (IBEM) are investigated. The detection of cracks is of interest because their presence may compromise structural elements, put technological devices at risk or represent economical potential in reservoir engineering. Shallow cracks may give rise to scattered body and surface waves. These waves are sensitive to the crack's geometry, size and orientation. Under certain conditions, amplitude spectra clearly show conspicuous resonances that are associated with trapped waves. Several applications based on the scattering of surface waves (e.g. Rayleigh and Stoneley waves), such as non-destructive testing or oil well exploration, have shown that the scattered fields may provide useful information to detect cracks and other heterogeneities. The subject is not new and several analytical and numerical techniques have been applied for the last 50 years to understand the basis of multiple scattering phenomena. In this work, we use the IBEM to calculate the scattered fields produced by single or multiple cracks near a free surface. This method is based upon an integral representation of the scattered displacement fields, which is derived from Somigliana's identity. Results are given in both frequency and time domains. The analyses of the displacement field using synthetic seismograms and snapshots reveal some important effects from various configurations of cracks. The study of these simple cases may provide an archetype to geoscientists and engineers to understand the fundamental aspects of multiple scattering and diffraction by cracks.

**Keywords:** wave propagation, multiple scattering, cracks, Rayleigh waves

## 1. Introduction

Cracks in solids are due to many causes. Among them are the material's fatigue or high stress concentrations. Commonly, their traces may appear at the free surface, but in most cases, fractures do not outcrop and inverse methods are then needed in order to be detected and measured. For example in oil reservoirs, fracture identification and characterization can be used to improve production. The fracture system may induce hydrocarbon accumulation and preferential permeability. Indeed, in well drilling such information is crucial because the drilling programming takes advantage of knowledge on the preferential direction of fractures. On the other hand, induced hydraulic fracturing is commonly performed to enhance hydrocarbon production; information on the geometry and distribution of induced fractures is essential for this purpose.

Although in theory the orientation, size and position of cracks can be inferred from wave propagation features under controlled experiments (Keer *et al* 1984), in practice the

  

situation is quite complicated because uncertainties and the ill-posed nature of the inverse problem allow one to only deal with extremely simple configurations. The scattering and diffraction of elastic waves by a single obstacle have been relevant issues in non-destructive evaluation techniques and geophysical prospecting for many years (Davis *et al* 2001). On shallow cracks, important wave interaction between the surface and cracks takes place and it is expected to give valuable information on their characterization from a frequency analysis (Achenbach *et al* 1983, 1984).

Nowadays, a variety of approaches are available to deal with almost any geometry and configuration. The monograph by Zhang and Gross (1998) represents a good starting point for an interested reader. Chen (1975) was the pioneer in the application of finite difference schemes to wave propagation problems in cracked media. His work deals with a bounded plate that contains a finite central crack excited by a rapid tension load. Excellent agreement was found with the analytical results of Baker (1962). At the end of the past century, Frangi (1998) and Rodríguez *et al* (1999) solved the same problem with the boundary element method and finite element method, respectively. They observed that the behaviour of the system is based on the wave interactions between plate boundaries and the crack surface. These interactions may induce significant stress concentrations and crack growth. For multiple scattering in 2D, Liu *et al* (1989, 1991, 1993) studied cross-hole surveys and vertical seismic profiling. They proposed effective medium models for the elastic wave propagation when the wavelengths are larger than the crack sizes. For wavelengths similar to the scatterer size, it is worth mentioning the work by Pointer *et al* (1998, 2000). Realistic scatterer configurations have been studied assuming fractal geometry distributions (Liu *et al* 1999, 2000, Liu and Zhang 2001). Recently, 2D numerical studies regarding cracked media were carried out by Iturrarán-Viveros *et al* (2005)) and Rodríguez-Castellanos *et al* (2006, 2007), where the application of the indirect boundary element method (IBEM) to wave propagation problems was evinced.

Studies in 3D are rare because of the inherent increased difficulties. However, under controlled circumstances, Kirchhoff's approximation allow for the modelling of scattering by cracks in the high frequency regime in order to infer crack sizes and shapes (Liu *et al* 1997). Other 3D recent studies are, for example, the asymptotic solutions of the dispersion equations in the long- and short-wavelength regimes by Kanaun *et al* (2004), the acoustic wave propagation by cylindrical shells (Veksler *et al* 2000, Cai 2004), the simulations of elastic wave propagation by 3D cracks using the indirect boundary element method (Iturrarán-Viveros *et al* 2008) and the elastic wave scattering by spheres (Ávila-Carrera and Sánchez-Sesma 2006, Videen 2003, Gritto *et al* 1995, 1999). Multiple 3D scattering has been dealt by Eriksson *et al* (1995) for a distribution of penny-shaped cracks and by Boström (1980) for a few scatterers.

In this paper, we study the scattering of Rayleigh waves by shallow cracks in a 2D configuration. We use the IBEM to solve a model which contains several near free-surface cracks. The IBEM was developed in the early 1990s with several successful applications to elastic wave propagation (Sánchez-Sesma and Campillo 1991, Sánchez-Sesma *et al* 1993, Sánchez-Sesma and Luzón 1995, Luzón *et al* 1997, Vai *et al* 1999). The method is based upon the integral representation of the scattered fields in terms of single-layer boundary sources, which is derived from Somigliana's identity. The formulation allows us to deal with multiple scattering, once the source is given and boundary conditions are enforced. Boundary conditions lead to Fredholm's integral equation of the second kind for the sources. A discretization scheme based on numerical and analytical integrations of the exact Green's functions for displacements and tractions is employed. The formulation presented here separate cracked from non-cracked responses. The total displacement field at the cracked half-space is taken as the superposition of both the specified incident field (e.g. Rayleigh-wave incidence) at the non-cracked half-space and the scattered field at the cracked one. On the free surface and crack faces, suitable traction conditions are held. Our results have been validated with those previously published by Achenbach *et al* (1983) (see Rodriguez-Castellanos *et al* (2005)) for a single flat crack parallel to the free surface under the incidence of P-waves. The agreement obtained is excellent. In order to illustrate wave-motion characteristics, frequency responses, synthetic seismograms and snapshots of the wave field for some relevant configurations are analysed. Time histories of the Rayleigh-wave incidence reveal important diffraction and attenuation. Conspicuous effects take place when the cracks have certain preferential conditions relative to the incidence. The results reported here correspond to those of multiple scattering problems at intermediate or high frequency regimes. We hope that this fundamental set of results could be useful to geoscientists and engineers who need to validate and calibrate their methods.

## 2. Integral representation

We use the IBEM based on the formulation given by Sánchez-Sesma and Campillo (1991). In the following, we summarize the main aspects of this formulation.

Let us consider a domain $V$ and its boundary $S$. If we suppose that the medium is elastic and linear, the displacement field under harmonic excitation can be written, neglecting body forces, by means of the single-layer boundary integral equation,

$$u_i(\mathbf{x}) = \int_S \phi_j(\boldsymbol{\xi}) G_{ij}(\mathbf{x}; \boldsymbol{\xi})\, \mathrm{d}S_\xi, \tag{1}$$

where $u_i(\mathbf{x})$ is the $i$th component of the displacement at point $\mathbf{x}$, $G_{ij}(\mathbf{x}; \boldsymbol{\xi})$ is the Green's function for a full space, which represents the displacement produced in direction $i$ at $\mathbf{x}$ due to the application of a unit force in direction $j$ at point $\boldsymbol{\xi}$, and $\phi_j(\boldsymbol{\xi})$ is the force density in direction $j$ at point $\boldsymbol{\xi}$.

From a limiting process based on equilibrium considerations around an internal neighbourhood of the boundary, it is possible to write, for $\mathbf{x}$ on $S$,

$$t_i(\mathbf{x}) = c\phi_i(\mathbf{x}) + \int_S \phi_j(\boldsymbol{\xi}) T_{ij}(\mathbf{x}; \boldsymbol{\xi})\, \mathrm{d}S_\xi, \tag{2}$$

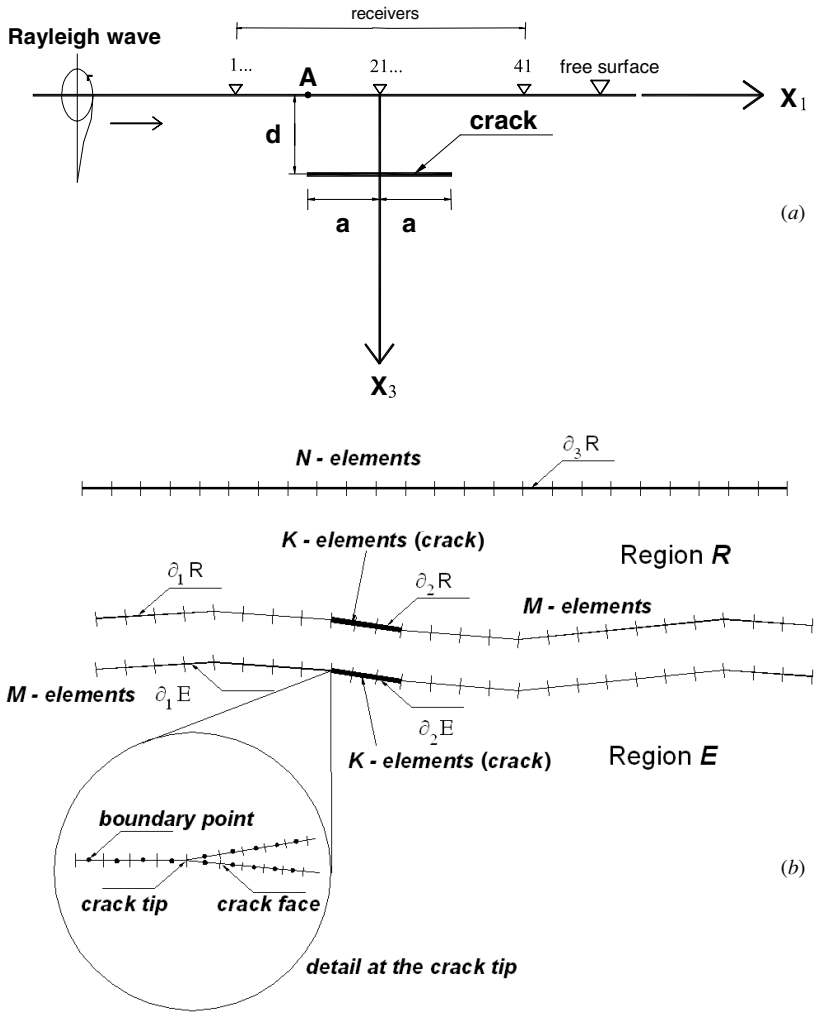


**Figure 1.** (*a*) Elastic half-space containing a shallow crack under the incidence of Rayleigh waves. (*b*) Configuration by regions $R$ and $E$ of the elastic half-space. The free surface is discretized in $N$ elements, the crack in $K$ elements and the common interface between $R$ and $E$ in $M$ elements.

where $t_i(\mathbf{x})$ is the $i$th component of traction, $c = 0.5$ if $\mathbf{x}$ tends to boundary $S$ from inside the region, $c = -0.5$ if $\mathbf{x}$ tends to $S$ from outside the region and $c = 0$ if $\mathbf{x}$ is not on $S$. $T_{ij}(\mathbf{x};\boldsymbol{\xi})$ is the traction Green's function for a full space. Green's functions for displacement and traction and additional details about equations (1) and (2) can be found, for instance, in Sánchez-Sesma and Campillo (1991).

## 3. Formulation of the problem

Considering the configuration shown in figure 1(*a*), we see that it is possible to divide the domain into two regions, $R$ and $E$ (figure 1(*b*)); here, adequate boundary conditions must be imposed. The fictitious interface between the regions $R$ and $E$ is used to handle with one or more discontinuities following the multi-region concept. Moreover, this interface allows us to use the Green's functions, by just taking into account the fact that no hypersingular integrals are considered. The scattering of elastic waves by cracks using the direct BEM leads to hypersingular integrals when imposing boundary conditions (tractions at the crack), and this is the subject of several works (e.g. Chen and Hong (1999) and Aliabadi (1997)). However, when the multi-region concept is invoked the solution of hypersingular integrals is not required. For the free surface ($\partial_3 R$), the traction-free boundary condition must be enforced $\left(t_i^R(\mathbf{x}) = 0\right)$. Similarly, the same condition should be applied to the crack's faces ($\partial_2 R$ and $\partial_2 E$). Tractions and displacements must be continuous at the interface between the two regions ($\partial_1 R = \partial_1 E$). Because of linearity, the total displacement and traction fields can be expressed by the superposition of the known *reference* solution (i.e. the analytical solution in the half-space without cracks or cavities) and the diffracted field, that is, $u = u^0 + u^{\mathrm{d}}$ and $t = t^0 + t^{\mathrm{d}}$, where the superscript 0 indicates the *reference* solution (i.e. Rayleigh waves) and d is the diffracted field obtained by means of our integral representation (equations (1) and (2)). These five conditions, respectively, allow us to write a system of integral equations for the unknown force densities:

$$c\phi_i^R(\mathbf{x}) + \int_{\partial R} \phi_j^R(\boldsymbol{\xi}) T_{ij}^R(\mathbf{x};\boldsymbol{\xi})\,\mathrm{d}S_\xi = -t_i^{0R}(\mathbf{x}), \quad \mathbf{x} \in \partial_3 R, \tag{3}$$

$$c\phi_i^R(\mathbf{x}) + \int_{\partial R} \phi_j^R(\boldsymbol{\xi}) T_{ij}^R(\mathbf{x};\boldsymbol{\xi})\,\mathrm{d}S_\xi = -t_i^{0R}(\mathbf{x}), \quad \mathbf{x} \in \partial_2 R, \tag{4}$$

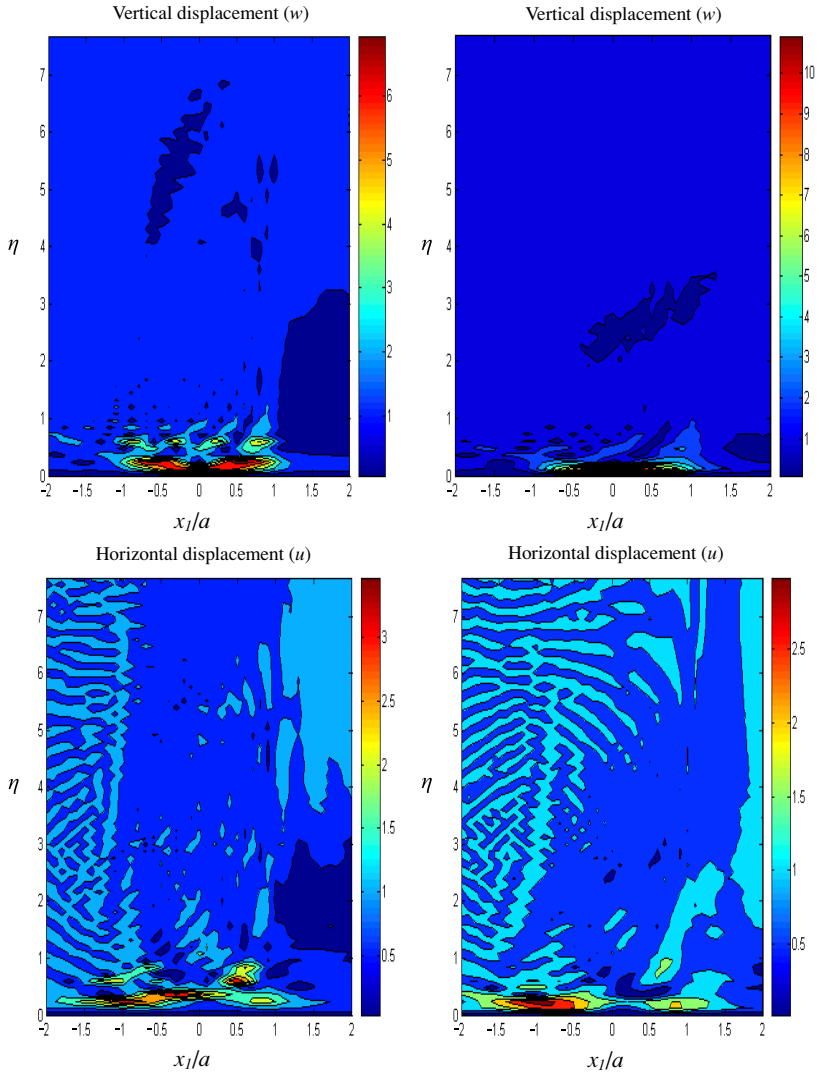


**Figure 2.** Frequency responses for the model of figure 1(*a*) showing the amplitude spectra of the transfer functions for shallow $d/2a = 0.2$ (left) and deeper $d/2a = 0.4$ (right) cracks.

$$c\phi_i^E(\mathbf{x}) + \int_{\partial E} \phi_j^E(\boldsymbol{\xi}) T_{ij}^E(\mathbf{x};\boldsymbol{\xi})\,\mathrm{d}S_\xi = -t_i^{0E}(\mathbf{x}), \quad \mathbf{x} \in \partial_2 E, \tag{5}$$

$$\int_{\partial R} \phi_j^R(\boldsymbol{\xi}) G_{ij}^R(\mathbf{x};\boldsymbol{\xi})\,\mathrm{d}S_\xi - \int_{\partial E} \phi_j^E(\boldsymbol{\xi}) G_{ij}^E(\mathbf{x};\boldsymbol{\xi})\,\mathrm{d}S_\xi = u_i^{0E}(\mathbf{x}) - u_i^{0R}(\mathbf{x}), \quad \mathbf{x} \in \partial_1 R = \partial_1 E, \tag{6}$$

and

$$c\phi_i^R(\mathbf{x}) + \int_{\partial R} \phi_j^R(\boldsymbol{\xi}) T_{ij}^R(\mathbf{x};\boldsymbol{\xi})\,\mathrm{d}S_\xi - c\phi_i^E(\mathbf{x}) - \int_{\partial E} \phi_j^E(\boldsymbol{\xi}) T_{ij}^E(\mathbf{x};\boldsymbol{\xi})\,\mathrm{d}S_\xi = t_i^{0E}(\mathbf{x}) - t_i^{0R}(\mathbf{x}), \quad \mathbf{x} \in \partial_1 R = \partial_1 E. \tag{7}$$

To numerically solve the system of integral equations (3)–(7), we discretize these appropriately. In general, the boundaries of each region are discretized into linear segments whose size depends on the shortest wavelength (six boundary segments per wavelength). The force densities $\phi$'s are taken to be constant along each segment and Gaussian integration (or analytical integration, where the Green's function is singular) is performed. The system to be solved is composed of $2(N + 2(M + K))$ equations, where $N$, $M$ and $K$ are defined in figure 1(*b*). Once the system of integral equations is solved, the unknown values of $\phi$'s are obtained and the diffracted displacement and traction fields are computed by means of equations (1) and (2), respectively. Additional details regarding the discretization procedure can be found in Rodríguez-Castellanos *et al* (2005).

The IBEM can be seen as the numerical realization of Huygens' principle. Therefore, to reconstruct a given wave front all points at the free surface and the continuous interface which act as sources and radiate energy must be taken into account. The truncation of the free surface induces artificial perturbations caused by diffractions at the edges of the model. However, these perturbations are characterized by small amplitudes and their reflections inside the model are negligible. The simplest solution is to choose a sufficiently large surface length for the fictitious perturbations fall outside

the observational spacetime window. We have observed that the free surface can be truncated at a distance '$a$' from both the left and right crack's tips. This criterion has shown good results; for instance, we were able to reproduce the correct diffracted wave field obtained by Achenbach *et al* (1983) (see Rodríguez-Castellanos *et al* (2005)). Additionally, this distance has been enough to avoid reflected waves from the left or right end of the free surface; this effect can be seen in all our time analysis.

## 4. Numerical results and discussion

In this section, various examples of wave propagation in media with cracks are analysed. We use incident surface Rayleigh waves to compute horizontal ($u$) and vertical ($w$) displacements.

Rayleigh waves in an elastic half-space correspond to a very special case of in-plane motion that involves coupled inhomogeneous plane P- and SV-waves propagating simultaneously at a speed that is lower than the respective wave propagation velocities $\alpha$ and $\beta$, for P- and S-waves, respectively. For a full treatment, see Achenbach (1973). Under the assumption of propagating harmonic plane waves and the enforcing of free surface boundary conditions, it is possible to write the incoming Rayleigh wave by means of

$$\begin{aligned} u^{0R}(x_1, x_3, \omega) &= \{\delta^2 \exp(-\mathrm{i}\gamma x_3) \\ &\quad + [1 - 2\delta^2] \exp(-\mathrm{i}\upsilon x_3)\} \exp\left(-\mathrm{i}\frac{\omega}{c_\mathrm{R}} x_1\right), \\ w^{0R}(x_1, x_3, \omega) &= \mathrm{i}\xi \{[1 - 2\delta^2] \exp(-\mathrm{i}\gamma x_3) \\ &\quad + 2\delta^2 \exp(-\mathrm{i}\upsilon x_3)\} \exp\left(-\mathrm{i}\frac{\omega}{c_\mathrm{R}} x_1\right), \end{aligned} \tag{8}$$

which correspond to horizontal and vertical ground motions, respectively. At the free surface of the half-space, the horizontal motion is a unit harmonic wave propagating at speed $c_\mathrm{R} < \beta < \alpha$. In these equations, $\delta = \beta/c_\mathrm{R}$, $\gamma^2 = \omega^2/\alpha^2 - \omega^2/c_\mathrm{R}^2$, $\upsilon^2 = \omega^2/\beta^2 - \omega^2/c_\mathrm{R}^2$, and $\xi = (2\delta^2 - 1)/(2\delta \times (\delta^2 - 1)^{1/2})$ is the so-called ellipticity. The vertical wavenumbers $\gamma$ and $\upsilon$ should be negative imaginary numbers to ensure decay with depth. $c_\mathrm{R}$ = Rayleigh wave velocity and $\omega$ = circular frequency.

The stress field associated with the incoming Rayleigh wave can be written as

$$\begin{aligned} \sigma_{xx}^{0R}(x_1, x_3, \omega) &= \mathrm{i}2\mu k \{[2\beta^2/\alpha^2 - 2\delta^2 - 1] \\ &\quad \times \exp(-\mathrm{i}\gamma x_3) + [2\delta^2 - 1] \exp(-\mathrm{i}\upsilon x_3)\} \exp\left(-\mathrm{i}\frac{\omega}{c_\mathrm{R}} x_1\right), \\ \sigma_{zz}^{0R}(x_1, x_3, \omega) &= \mathrm{i}2\mu k (2\delta^2 - 1) \{\exp(-\mathrm{i}\gamma x_3) \\ &\quad - \exp(-\mathrm{i}\upsilon x_3)\} \exp\left(-\mathrm{i}\frac{\omega}{c_\mathrm{R}} x_1\right), \\ \sigma_{xz}^{0R}(x_1, x_3, \omega) &= -\mu \frac{\omega}{\beta} \frac{(2\delta^2 - 1)^2}{(\delta^2 - 1)^{1/2}} \{\exp(-\mathrm{i}\gamma x_3) \\ &\quad - \exp(-\mathrm{i}\upsilon x_3)\} \exp\left(-\mathrm{i}\frac{\omega}{c_\mathrm{R}} x_1\right). \end{aligned} \tag{9}$$

We can see that the normal and shear stresses are null at the free surface. In these equations, $\mu$ = shear modulus and $k = \omega/c_\mathrm{R}$.

We consider primarily two cases: $d/2a = 0.2$ and 0.4. A maximum normalized frequency $\eta = 2\, a/\lambda_\mathrm{S} = 7.68$, where

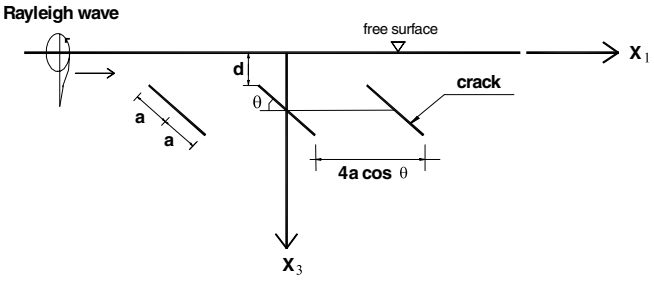


**Figure 3.** Elastic half-space containing three cracks under the incidence of Rayleigh waves.

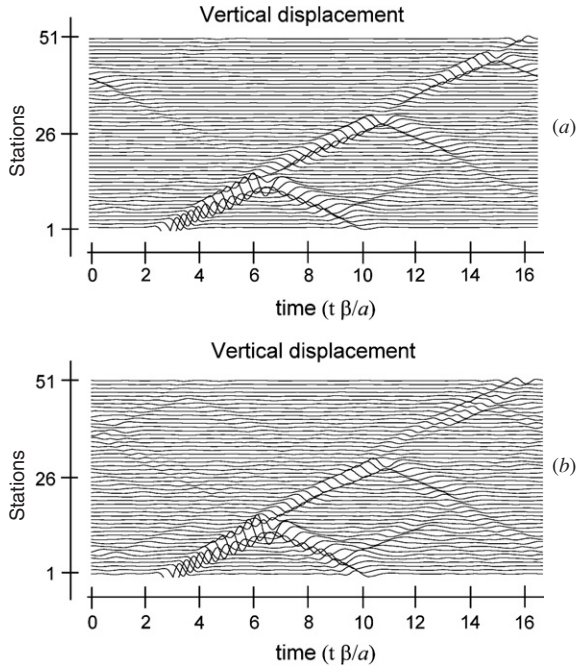


**Figure 4.** Synthetic seismograms computed for the model of figure 3. Vertical displacements are plotted for two cases: (*a*) three horizontal cracks ($\theta = 0^\circ$) with $Q = 25$ and (*b*) three horizontal cracks ($\theta = 0^\circ$) with $Q = 250$. Incidence of surface Rayleigh waves.

$\lambda_\mathrm{S}$ stands for the minimum shear wavelength. Poisson's ratio is $\nu = 0.3$. P- and S-wave quality factors were considered constants. The values used here are $Q_\mathrm{P} = Q_\mathrm{S} = Q = 25$ and 50. This is made to adequately introduce hysteretic damping by using the factor $(1 - \mathrm{i}/2Q)$. We obtained results for 64 frequencies at 41 or 51 receivers located on the free surface. The minimum and maximum frequencies employed for computations were $\eta = 0$ and $\eta_\mathrm{max} = 7.68$ respectively and a sampling frequency of $\Delta\eta = 0.12$. For the computation of the transient response, we employ a maximum frequency $\eta = 2a/\lambda_\mathrm{S} = 7.68$. In order to simulate wave propagation along time, we adopt the FFT algorithm to calculate synthetic seismograms and snapshots using the Ricker wavelet as the source signal with a normalized characteristic period $t_\mathrm{p}\beta/a = 1$.

The frequency response of the incoming surface Rayleigh waves is illustrated in figure 2. The vertical ($w$) (top) and horizontal ($u$) (bottom) components of displacement for the model of figure 1(*a*) are displayed. The spectra of the transfer

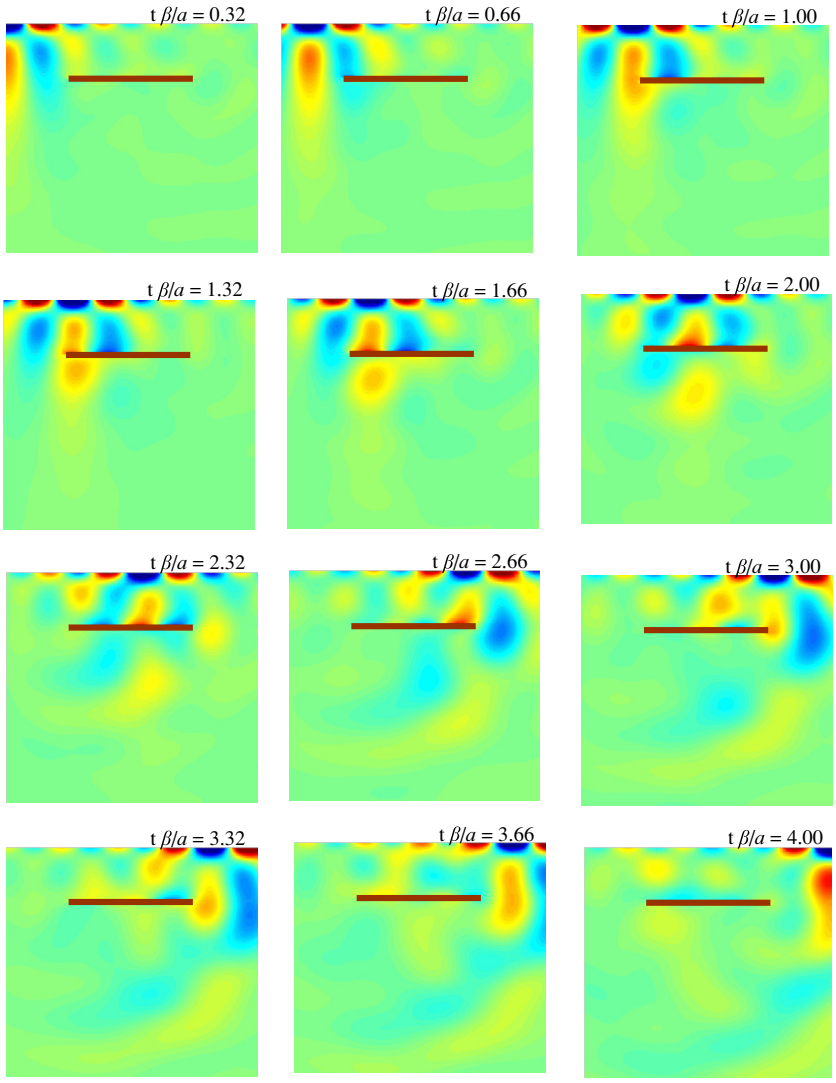


**Figure 5.** Snapshots for the model of figure 1(*a*).

functions for shallow $d/2a = 0.2$ (left) and deeper $d/2a = 0.4$ (right) cracks are shown. Forty-one equidistant receivers were located at the free surface ranging from $x_1/a = -2$ to $x_1/a = 2$. The following values were employed to perform the computations in the frequency domain: $\nu = 0.3$, $Q_{\mathrm{P}} = Q_{\mathrm{S}} = Q = 50$, 64 frequencies with $\Delta\eta = 0.12$ and a maximum frequency of $\eta_{\max} = 7.68$.

The information provided by the frequency response of the models is of much interest. As can be seen in figure 2, the interaction of the incoming Rayleigh-wave field appears to be more sensitive to the horizontal component of displacement than to the vertical one. It is easy to observe aligned patterns of high frequency modes provoked by the interaction of the incoming field and the crack. These aligned frequency structures are called diffraction patterns. At low-frequency regimes, the transfer functions elucidate to the 1D layer frequency response, which is described by $a/2d$. This quantity corresponds to the fundamental mode of the equivalent single layer conformed by the upper crack face and the free surface. On the other hand, it is remarkable that in the vertical component spectra, stronger amplitudes rapidly decay as the frequency increases. Conspicuous resonant peaks are observed at low frequencies produced by the interaction of the incident wave field and the shallow crack. Such peaks are symmetric and they are correlated with the maximum spectral ordinates of the model. Similar behaviour is shown by the vertical component response for the deeper crack. In general, a rapid attenuation effect is observed from low to high frequency at all cases. This relevant fact will be discussed in detail in further examples and we will also include analyses in the time domain.

It is important to remark that we use the same values for the fraction of damping $Q$ of both P- and S-waves, that is, $Q_{\mathrm{P}} = Q_{\mathrm{S}} = Q = 50$. This is made to adequately introduce hysteretic damping by using the factor $(1 - \mathrm{i}/2Q)$. This is an attenuation approach that depends on the viscosity of the medium and does not depend on the frequency. Such modification is introduced during the computations of the compressional and shear wave numbers respectively. These quantities are now complex and are of much help to avoid noise problems in the construction of time responses.

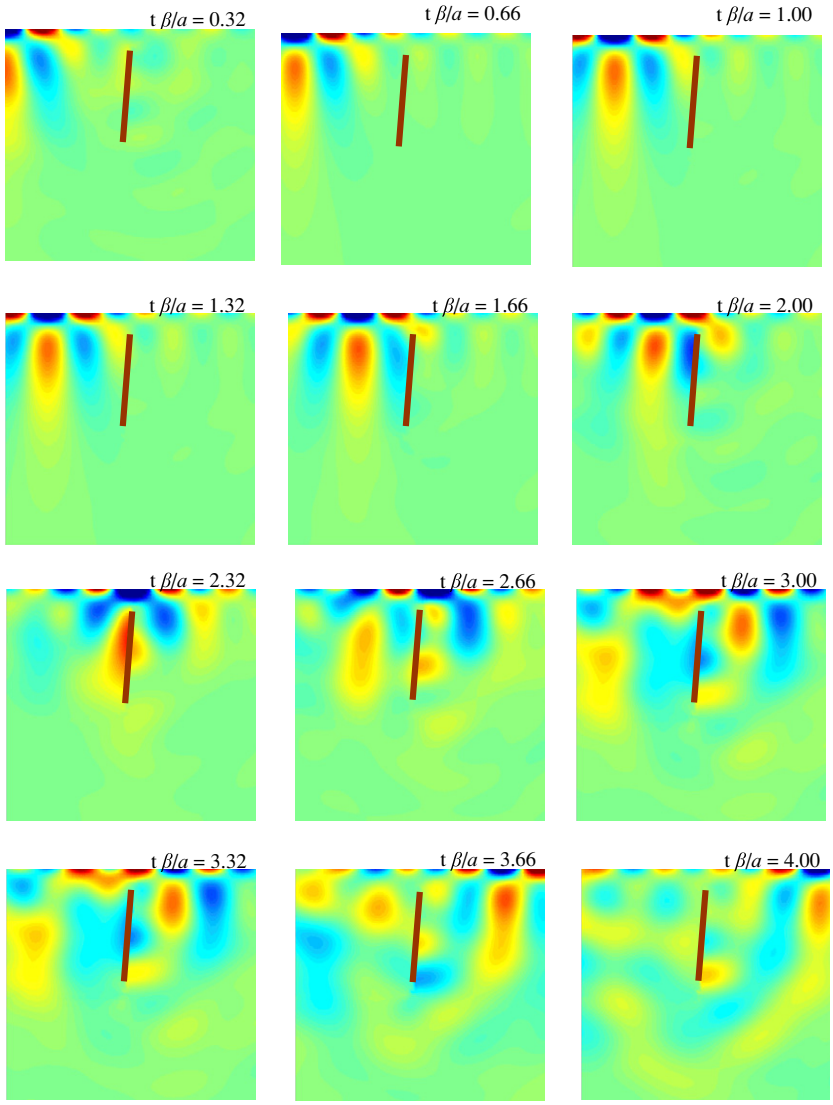


**Figure 6.** Snapshots of a single vertical crack.

In figure 3, a multiple scattering configuration for three dipping cracks under the incidence of Rayleigh waves is illustrated. Here, we considered two examples and the same physical parameters as those of figure 2. The first case corresponds to three horizontal cracks with $\theta = 0^\circ$, localized at depth $d/2a = 0.2$; the second configuration considers three dipping cracks with $\theta = 60^\circ$, each one at depth $d/2a = 0.1$. For the first case, figure 4 illustrates an example where the two fields (damped and undamped) are compared. Here, only vertical displacements are depicted for cases $(a)$ $\theta = 0^\circ$ and $Q = 25$ and $(b)$ $\theta = 0^\circ$ and $Q = 250$. Fifty-one equally spaced receivers were located at the free surface from $x_1/a = -6$ to $x_1/a = 6$. In case $(a)$, the presence of the shallower set of horizontal cracks produces a very clean (not noise) scattering pattern than in case $(b)$, which corresponds to an undamped case. Each horizontal crack produces the emission of a diffracted wave-front travelling backwards to the surface. The incoming surface wave appears to be attenuated due to a sequential interaction among the cracks.

On the other hand, synthetic seismograms for the undamped case (figure 4$(b)$) appear to be noisy. This is the result of travelling energy that reappears at the beginning of the seismogram due to the so-called aliasing effect. This phenomenon is generated at the moment of the computation of the Fourier transpose and it preserves the continuity of energy that has not been attenuated given the high value of the fraction of damping $Q_P = Q_S = Q = 250$. Similar effect is clearly seen for the damped case of figure 4$(a)$, but only for the prominent first reflection of the Rayleigh wave and the first crack. We must clarify that no smooth operator has been applied for the plots. Several examples for $Q = 500$ and 5000 were performed but are not depicted in this work.

In order to observe and describe the Rayleigh-wave motion over the entire model, a set of snapshots for the displacement field have been displayed. In figures 5 and 6, square arrays of 51 receivers with $\mathrm{d}x_1/a = \mathrm{d}x_3/a = 0.08$ for 12 times $(0.32 \leqslant t\beta/a \leqslant 4.0)$ of propagation are shown. $\nu = 0.3$, $Q_P = Q_S = Q = 50$, 64 frequencies with $\Delta\eta = 0.12$ and a maximum frequency of $\eta_{\max} = 7.68$ were used

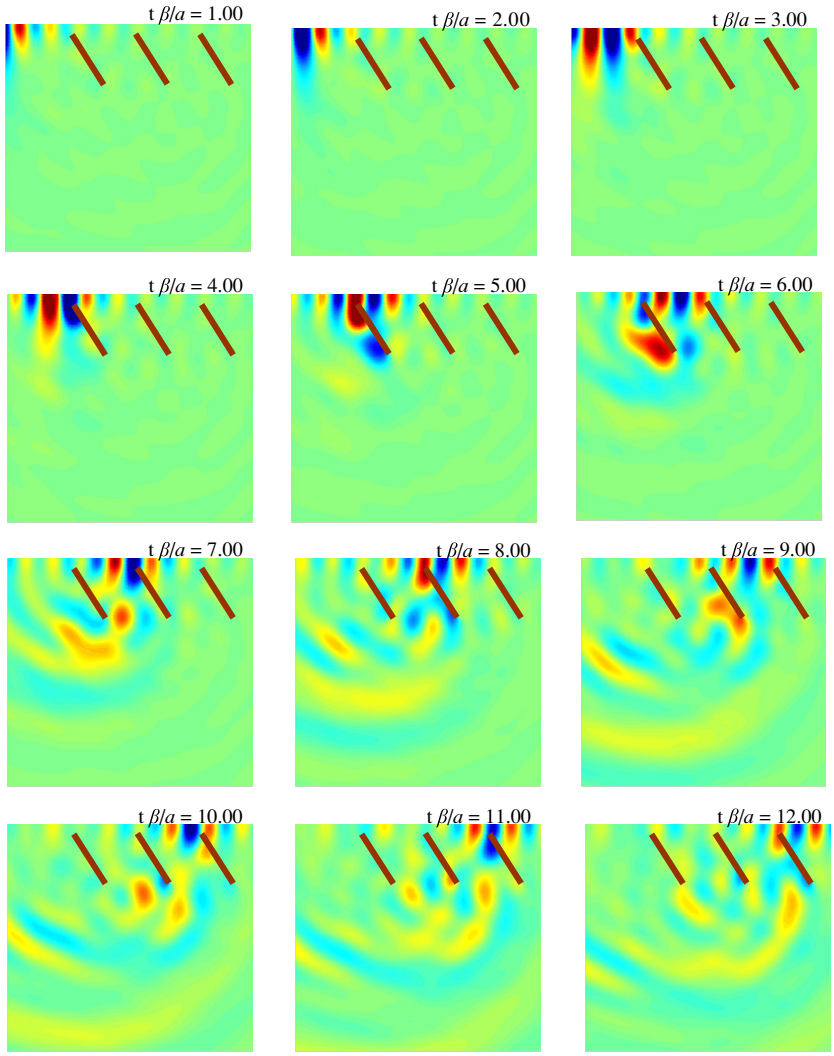


**Figure 7.** Snapshots for the model given in figure 3.

for computations in the frequency domain. Figure 5 sketches only the horizontal displacements ($u$) produced by a single horizontal crack of figure 1($a$) at normalized depth $d/2a = 0.5$. The diffracted waves from the crack tip are significant around the dimensionless time $t\beta/a = 1.0$. While the horizontal position of the crack only affects the incident Rayleigh-wave amplitude at that depth, a partition of energy and scattering is clearly generated. Here, the crack acts like a separator of energy. The incident wave field travels horizontally with no attenuation between the free surface and the upper face of the crack. On the lower face of the crack, a shadow effect and scattering patterns travelling to the bottom of the model are easily displayed. In figure 6, the transient response of a single crack oriented with $\theta = 100^{\circ}$ at relative depth $d/2a = 0.1$ is evaluated. The incident Rayleigh wave is greatly reflected and a partial amount of energy is scattered by the presence of the crack. We must mention that the incoming field is strongly attenuated once the interaction with the crack has taken place. For this example, the crack behaves like a barrier of waves, provoking the disappearance of the wave field and marked shadow zones at the opposite side of the incidence.

In figure 7, we use the same properties and physical parameters as those reported in figure 4($b$). Computations were performed for three dipping cracks located at depth $d/2a = 0.1$. Here, the vertical displacement field ($w$) for 12 times ($1 \leqslant t\beta/a \leqslant 12$) of movement is displayed. A regular square grid of 51 receivers with $\mathrm{d}x_1/a = \mathrm{d}x_3/a = 0.24$ was used for computations. It is clear that the reflections provoked by the periodic appearance of cracks redirect the incident wave energy to the bottom of the medium. The system of cracks acts like a deviator of waves. The shadow effects caused by both the position and orientation of cracks tend to diminish the wave amplitude, just right before the next crack interaction occurs. At the free surface, this opposite orientation of the cracks acts over the incident wave field to be poorly measured at the last set of receivers. The remaining field recorded at the last group of receivers corresponds to a distorted Rayleigh wave, a wave reduced in amplitude and hard to identify. Thus, a strong attenuation effect and a weak response of the reflected and diffracted pulses by the crack system are well observed as time passes. In several engineering problems, this effect may cause troubles on the incident field recognition after its interaction with a

heterogeneous medium. In some instances with abundant cracks, the source field is completely lost. In a contrary case, when the cracks are placed in a proper orientation to reflect energy towards the free surface, a strong local amplification effect may occur.

## 5. Conclusions

In the present work, we employ the indirect boundary element method (IBEM) to study the multiple scattering and seismic response of an elastic medium that contains a single or several cracks under the incidence of Rayleigh waves. This numerical technique, which is based upon an integral representation of the diffracted wave field, can be seen as a numerical realization of Huygens's principle, since diffracted waves are constructed at the boundaries of cracks from where they are radiated. As a reference to the validation and the applicability of the IBEM to the problem of elastic wave propagation in media with cracks, the results for P- and S-waves were published in a previous paper (Rodríguez-Castellanos *et al* 2005). From the single scatterer results, we have shown here that the crack behaves as a separator of waves and, at the same time, produces the emission of diffracted energy which is observed at the receivers on the free surface. Additionally, it has been pointed out that the crack appears to be less effective to trap energy when it is located far from the free surface. In the vertical position of the single crack it has been shown that the incident Rayleigh wave is greatly reflected. A partial amount of energy is scattered to the shadow side of the crack and a strong attenuation effect over the incident wave field takes place. It is clearly observed that the crack behaves like a barrier of waves, provoking the disappearance of the wave field and marked shadow zones at the opposite side of the incidence.

From multiple scattering results at an intermediate frequency regime, we have found that near free-surface cracks influence the propagation of Rayleigh waves. In fact, it is well known that a major amount of energy from Rayleigh waves is located around the free surface. The evidence of such a phenomenon is evinced by the frequency–space spectral plots. In this sense, near free-surface cracks may produce different attenuation factors depending on which (horizontal or vertical) component of movement is measured. Another important aspect that we must remark is related to the orientation of cracks. The cracks' relative position among each other and with respect to the free surface is crucial to understanding attenuation and anisotropy. When the cracks are placed parallel to the free surface, the emission of diffracted waves from the crack travelling backwards to the surface is observed. For dipping cracks, the displacements observed at the free surface have less energy due to the significant reorientation of energy and strong diffraction emitted to the interior of the medium. We must remark that in various engineering and geophysical problems, this effect may cause trouble in the incident field recognition after its interaction with an unknown heterogeneous medium. In some cases, the interaction of the incident field with a complex medium may cause dominant effects over the wave propagation and lead to the loss, or to the amplification, of the original signal.

The simple models presented in this work have the aim of showing the complexity of propagation and multiple scattering of elastic waves by cracks. Our purpose is to offer a way of comparison and validation of results obtained by other new techniques. The set of results reported here show quantitatively the frequency and transient response of surface wave propagation phenomena in computational models with cracks. More complicated models including a growing number of scatterers with several distributions and shapes are a subject of future research. However, we believe that a strong need of analytical and numerical formulations to solve multiple scattering problems at intermediate or high frequencies is still present. The correct interpretation of real data in the petroleum field, in geophysical applications, in non-destructive tests and the calibration of modelling techniques are some areas of science and engineering that require benchmark and trustworthy solutions as reported here.

## Acknowledgments

We would like to thank Jim Spurlin for his valuable comments and critical reading of the manuscript. This work was partially supported by Instituto Mexicano del Petróleo, under Geophysical Prospecting Department, Geophysical Exploration and Exploitation Research Program under project D.00393 and Civil Engineering Department and by CONACYT, México, under grant NC204 and by DGAPA-UNAM, México, under Project IN121709.

## References

Achenbach J D 1973 *Wave Propagation in Elastic Solids* (Amsterdam: North-Holland)

Achenbach J D, Angel Y C and Lin W 1984 Scattering from surface-breaking and near-surface cracks *Wave Propagation in Homogeneous Media and Ultrasonic Nondestructive Evaluation* ed G C Johnson (New York: The American society of Mechanical Engineers) AMD 62:93

Achenbach J D, Lin W and Keer L M 1983 Surface waves due to scattering by a near-surface parallel crack *IEEE Trans. Sonics Ultrason.* **SU-30** 270

Aliabadi M H 1997 Boundary element formulations in fracture mechanics *Appl. Mech. Rev.* **50** 83–96

Ávila-Carrera R and Sánchez-Sesma F J 2006 Scattering and diffraction of elastic P- and S-waves by a spherical obstacle: a review of the classical solution *Geofís. Int.* **45** 3–21

Baker B R 1962 Dynamic stresses created by a moving crack *Trans. ASME* E **29** 449–58

Boström A 1980 Multiple scattering of elastic waves by bounded obstacles *J. Acoust. Soc. Am.* **67** 399–413

Cai L W 2004 Scattering of antiplane shear waves by layered circular elastic cylinder *J. Acoust. Soc. Am.* **115** 515–22

Chen J T and Hong H K 1999 Review of dual boundary element methods with emphasis on hypersingular integrals and divergent series *Appl. Mech. Rev.* **52** 17–32

Chen Y M 1975 Numerical computation of dynamic stress intensity factor by a Lagrangian finite-difference method (the HEMP Code) *Eng. Fract. Mech.* **7** 653–60

Davis C A, Lee V W and Bardet J P 2001 Transverse response of underground cavities and pipes to incident SV waves *Earth Eng. Struct. Dyn.* **30** 383–410

Eriksson A S, Boström A and Datta S K 1995 Ultrasonic wave propagation through a cracked solid *Wave Motion* **22** 297–310

Frangi A 1998 Some developments in the symmetric Galerkin boundary element method *PhD Thesis* Politecnico de Milano

Gritto R, Korneev V A and Johnson L R 1995 Low frequency elastic wave scattering by an inclusion: limits of applications *Geophys. J. Int.* **120** 677–92

Gritto R, Korneev V A and Johnson L R 1999 Nonlinear three-dimensional inversion of low frequency scattered elastic waves *Pure Appl. Geophys.* **156** 557–89

Iturrarán-Viveros U, Sánchez-Sesma F J and Luzón F 2008 Boundary element simulation of scattering of elastic waves by 3-D cracks *J. Appl. Geophys.* **64** 70–82

Iturrarán-Viveros U, Vai R and Sánchez-Sesma F J 2005 Scattering of elastic waves by a 2-D crack using the indirect boundary element method (IBEM) *Geophys. J. Int.* **162** 927–34

Kanaun S K, Levin V M and Sabina F J 2004 Propagation of elastic waves in composites with random set of spherical inclusions (effective medium approach) *Wave Motion* **40** 69–88

Keer L M, Lin W and Achenbach J D 1984 Resonance effects for a crack near a free surface *J. Appl. Mech.* **51** 65

Liu E, Crampin S and Booth D C 1989 Shear-wave splitting in cross-hole surveys: modeling *Geophysics* **54** 57–65

Liu E, Crampin S and Hudson J A 1997 Diffraction of seismic waves by cracks with application to hydraulic fracturing *Geophysics* **62** 253–65

Liu E, Crampin S and Queen J H 1991 Fracture detection using crosshole surveys and reverse vertical seismic profiles at the Conoco Borehole Test Facility Oklahoma *Geophys. J. Int.* **107** 449–63

Liu E, Crampin S, Queen J H and Rizer W D 1993 Velocity and attenuation anisotropy caused by micrographs and macrofractures in a multiazimuthal reverse VSP *Can. J. Expl. Geophys.* **29** 177–88

Liu E, Queen J H, Zhang Z and Chen D 2000 Simulation of multiple scattering of seismic waves by spatially distributed inclusions *Sci. China* E **43** 4

Liu E and Zhang Z 2001 Numerical study of elastic wave scattering by cracks or inclusions using the boundary integral equation method *J. Comp. Acoust.* **9** 1039–54

Liu E, Zhang Z and Niu B 1999 BEM simulation of multiple scattering of elastic waves by cracks *Proc. Int. Conf. on Bound. Elem. Tech. (Queen Mary College University of London)* ed M H Aliabadi pp 59–66

Luzón F, Sánchez-Sesma F J, Rodríguez-Zuñiga J L, Posadas A M, García J M, Martín J, Romacho M D and Navarro M 1997 Diffraction of P SV and Rayleigh waves by three-dimensional topographies *Geophys. J. Int.* **129** 571–8

Pointer T, Liu E and Hudson J A 1998 Numerical modeling of seismic waves scattered by hydrofractures: application of the indirect boundary element method *Geophys. J. Int.* **135** 289–303

Pointer T, Liu E and Hudson J A 2000 Seismic wave propagation in cracked porous media *Geophys. J. Int.* **142** 199–231

Rodríguez A, Hernández L H, Sánchez-Sesma F J and Urriolagoitia G 1999 Evaluación del factor de intensidad de esfuerzos bajo condiciones de carga dinámica *International Materials Research Congress (Cancún, México)*

Rodríguez-Castellanos A, Ávila-Carrera R and Sánchez-Sesma F J 2007 Scattering of Rayleigh-waves by surface-breaking cracks: an integral formulation *Geofís. Int.* **46** 241–8

Rodríguez-Castellanos A, Luzón F and Sánchez-Sesma F J 2005 Diffraction of seismic waves in an elastic cracked half-plane using a boundary integral formulation *Soil Dyn. Earth Eng.* **25** 827–37

Rodríguez-Castellanos A, Sánchez-Sesma F J, Luzón F and Martin R 2006 Multiple scattering of elastic waves by subsurface fractures and discontinuities *Bull. Seismol. Soc. Am.* **96** 1359–74

Sánchez-Sesma F J and Campillo M 1991 Diffraction of P, SV and Rayleigh waves by topographic features; a boundary integral formulation *Bull. Seismol. Soc. Am.* **81** 1–20

Sánchez-Sesma F J and Luzón F 1995 Seismic response of three-dimensional alluvial valleys for incident P, SV and Rayleigh waves *Bull. Seismol. Soc. Am.* **85** 269–84

Sánchez-Sesma F J, Ramos-Martínez J and Campillo M 1993 An indirect boundary element method applied to simulate the seismic response of alluvial valleys for incident P, SV and Rayleigh waves *Earth Eng. Struct. Dyn.* **22** 279–95

Vai R, Castillo-Covarrubias J M, Sánchez-Sesma F J, Komatitsch D and Vilotte J P 1999 Elastic wave propagation in an irregularly layered medium *Soil Dyn. Earth Eng.* **18** 11–8

Veksler N D, Lavie A and Dubus B 2000 Peripheral waves generated in a cylindrical shell with hemispherical end caps by a plane acoustic wave at axial incidence *Wave Motion* **4** 349–69

Videen G 2003 Seismic scattering from a spherical inclusion eccentrically located within a homogeneous spherical host: theoretical derivation *Waves Random Media* **13** 177–90

Zhang C and Gross D 1998 *On Wave Propagation in Elastic Solids with Cracks* (Southampton: Computational Mechanics Publications)